Lidar ratio calculations from in situ aerosol optical, microphysical and chemical measurements: Observations at puy de Dôme, France and analysis with CALIOP

Kruthika Eswaran, Nadège Montoux, Aurélien Chauvigné, Jean-Luc Baray, Gérard Ancellet, Karine Sellegri, Evelyn Freney, Clémence Rose, Jacques Pelon

Atmospheric Research 296 (2023) 107043

Contents lists available at ScienceDirect

Atmospheric Research

journal homepage: www.elsevier.com/locate/atmosres

Lidar ratio calculations from in situ aerosol optical, microphysical and chemical measurements: Observations at puy de Dôme, France and analysis with CALIOP

Kruthika Eswaran [a], Nadège Montoux [a,*], Aurélien Chauvigné [b], Jean-Luc Baray [a,c], Gérard Ancellet [d], Karine Sellegri [a], Evelyn Freney [a], Clémence Rose [a], Jacques Pelon [d]

[a] Université Clermont Auvergne, CNRS, Laboratoire de Météorologie Physique, UMR 6016, Clermont-Ferrand, France
[b] Laboratoire d'Optique Atmosphérique, UMR CNRS 8518, Université de Lille, Lille, France
[c] Université Clermont Auvergne, CNRS, Observatoire de Physique du Globe de Clermont Ferrand, UAR 833, Clermont-Ferrand, France
[d] LATMOS/IPSL, UPMC Univ. Paris 06 Sorbonne Universités, UVSQ, CNRS, Paris, France

ARTICLE INFO

Keywords:
Aerosols
Lidar ratio
CALIOP
In situ measurements

ABSTRACT

The ratio between lidar extinction and backscatter coefficients, also known as lidar ratio (LR), is an important parameter in atmospheric aerosol studies. In this paper, we propose a method to determine the 532 nm LR using in situ measurements performed over the 2015–2016 period at the puy de Dôme (PUY) station, central France, located at about 1465 m altitude. This method uses a Mie code with the measured aerosols size distribution and refractive index determined from aerosols optical measurements as inputs. The LR values obtained have been compared to LR calculated also with a Mie code but with refractive index determined from the measured aerosol chemical composition. A good correlation is observed for the period 2015–2016 with an agreement which increases to 99% after a significant imaginary part refractive index reduction, corresponding to much less carbonated particles than initially estimated. >50% of the LR values calculated at the station are within the 60–80 sr range under ambient atmospheric conditions. A statistical comparison with the CALIOP spatial lidar retrieval gives a good agreement at the location of PUY between retrieved values (62 sr) with a negligible bias and a dispersion indicative of a similar variability of LR (about 14 sr). The influence of air mass history on the LR has also been studied using backward trajectory analysis and CALIOP aerosol types along the trajectories, identifying five source regions. For continental, smoke and polluted dust aerosols types, CALIOP and PUY LR show a good agreement. For dusty and mainly clean marine aerosols, the differences observed between both suggest that air masses coming from the Atlantic Ocean sector at altitudes lower than 2.5 km, have experienced mixing with continental air masses during their travel increasing their LR before reaching the PUY station.

1. Introduction

Atmospheric aerosol particles affect the Earth's climate by influencing the radiation balance (Forster et al., 2021): they can absorb and scatter solar radiation, influence the properties of clouds, and affect precipitation (Tao et al., 2012). In addition, they also play a role in atmospheric chemistry and Earth's ecosystems (Pye et al., 2020). Quantifying the impact of aerosols with high confidence is a challenge given the spatial and temporal variability in their physical and chemical properties (Wang et al., 2015).

LIDAR (LIght Detection and Ranging) is a powerful remote sensing instrument for observing and studying the vertical structure of the atmosphere. To study the aerosol variability at global scale, spatial lidars as CALIOP onboard CALIPSO offer a good spatial coverage but provide only the aerosols optical properties as backscatter, extinction, aerosol optical depth (Winker et al., 2010; Liu et al., 2008). In situ measurements allow to retrieve some properties as chemical composition, size distribution, absorption and scattering coefficients at high temporal resolution however they cannot be directly compared to the spatial products. Methodologies have been developed to allow this comparison

* Corresponding author at: Laboratoire de Météorologie Physique, Université Clermont-Auvergne, Campus Universitaire des Cézeaux, 4 Avenue Blaise Pascal, TSA 60026, CS 60026, 63178 Aubière cedex, France.
E-mail address: nadege.montoux@uca.fr (N. Montoux).

https://doi.org/10.1016/j.atmosres.2023.107043
Received 7 July 2023; Received in revised form 16 September 2023; Accepted 3 October 2023
Available online 7 October 2023

notably for the lidar ratio (LR), i.e. the ratio between the aerosol extinction and backscatter coefficients. LR is an intensive property which depends on the particle size distribution, shape, refractive index and relative humidity (Evans, 1988). The characterization of the LR of different types of aerosols has been performed using direct measurements as with high spectral resolution lidar (Groß et al., 2013; Burton et al., 2012) and Raman lidar (Tesche et al., 2009; Müller et al., 2007) or by coupling elastic lidar with sun photometer (Wang et al., 2020; Pedros et al., 2010). Pedros et al. (2010) retrieved LR by iteratively tuning it to reconstruct sun-photometer AOD and further constrained it using air-mass trajectories from a Lagrangian trajectory model. LR can also be calculated indirectly with a Mie code using as inputs the aerosol size distribution and the refractive index. The code retrieves both extinction and backscatter coefficients which can then be used to calculate the LR. The inputs of the Mie code can be determined by different manners. For example, Cattrall et al. (2005) use sky and solar radiances at different wavelengths from the AERONET network while Masonis et al. (2003) use measured aerosol size distributions with a fixed refractive index to study marine aerosols. Alternatively, LR can be calculated as a function of aerosol single scattering albedo and the scattering phase function at 180° as Bréon (2013) did from POLDER/PARASOL passive satellite reflectance measurements at different wavelengths and in different directions. The aim of this paper is to use the in situ long-term measurements available at the mid-altitude puy de Dôme station (PUY) to calculate LR and study the difference in LR observed according to air mass origins. The different instruments available on the station allow to measure the aerosol size distribution and to determine the refractive index needed for Mie calculations. Its will allow in the future to better characterise the aerosols observed at PUY by combining chemical, microphysical and optical properties measured by in situ instruments with multiwavelength lidar measurements which start to be available since end of 2022 11 km far from PUY, LR being the common parameter for comparison.

The PUY station is a mid-altitude (1465 m.a.s.l) atmospheric observatory located in central France (45.77°N, 2.96° E), recognized as a global station of the GAW (Global Atmosphere Watch) network and is part of the instrumented platform for atmospheric research CO-PDD (Cézeaux-Aulnat-Opme Puy de Dôme). The aerosol and gas measurement series are now up to 25 years (Baray et al., 2020). Chauvigné et al. (2016) compared the aerosol optical properties and size distribution from in situ measurements with those measured in parallel by a sun-photometer. They concluded that the PUY station is representative of the total atmospheric column and regional conditions. Venzac et al. (2009) and more recently Laj et al. (2020) studied the seasonal analysis of climate-relevant in situ aerosol properties at several sites of the GAW network including PUY, showing that aerosol number concentration at PUY station, presents an annual cycle with a maximum during summer. The station can be influenced by local and regional pollution of continental nature. The different aerosol types detected at PUY affect the aerosol physical and optical properties measured implying a possible difference in the LR.

In the current study, the method developed uses a Mie code iteratively for the calculation of aerosol optical properties (Raut and Chazette, 2007). The LR values are then combined with a detailed back trajectory analysis and the CALIOP LR values, to study the influence of air mass history on the calculated LR.

2. Site and instruments description

2.1. The PUY station and its instruments

Measurements of various atmospheric parameters including aerosols, clouds and gases are performed continuously at the PUY station. In particular, the optical properties of aerosols (scattering, absorption) are measured in parallel to their size distribution over the sub and super micron ranges, and in parallel to the chemical composition of the submicron refractory aerosol (Mätzler, 2002). These measurements are operated in the European framework of ACTRIS (Aerosol Cloud and Trace gases Research Infrastructure). The instruments sample aerosol particles through a whole air inlet under both cloudy and clear-sky conditions. These inlets are designed to sample aerosol particles and cloud droplets, whose diameters are <30 μm, at a wind speed of 7 $m.s^{-1}$. The gradient between ambient and room temperature keeps the relative humidity at the inlet below 40%, ensuring the sampling of aerosol particles under dry conditions (Baray et al., 2020; Chauvigné et al., 2016).

2.1.1. Number particle size distribution

Sub-micron particles with diameters between 10 and 650 nm are measured using a custom made SMPS (Scanning Mobility Particle Sizer). Larger particles from 350 nm up to 17.5 μm are sampled by an OPC (Optical Particle Counter, Grimm model 1.108) (Burkart et al., 2010). To calculate the lidar ratio, we combine the measurements of both instruments (10 nm–420 nm for SMPS and 450 nm-17.5 μm for OPC) to get a size distribution from 10 nm to 17.5 μm with 116 bins.

2.1.2. Optical properties

The aerosol absorption and scattering coefficients are measured using a MAAP (Multi-Angle Absorption Photometer) and a nephelometer (TSI 3563), respectively. The MAAP retrieves the absorption coefficient at 670 nm by measuring the radiation transmitted and backscattered by particles loaded on a filter (Petzold and Schönlinner, 2004). The three-wavelength nephelometer (450, 550 and 700 nm) measures the scattering of light by aerosols at angles from 7° to 170° and light backscattered from 90° to 170°. The nephelometer data is corrected using correction factors according to Müller et al. (2011).

2.1.3. Chemical composition

The ACSM-ToF (Aerosol Chemical Speciation Monitor with a Time-of-Flight, Aerodyne) mass spectrometer measures the chemical composition of the submicron non-refractory fraction of the aerosol population, providing detection of the organic and inorganic species (e.g., NO_3^-, SO_4^{2-}, NH_4^+, and Cl^-) in real time (Fröhlich et al., 2013). At PUY, the Cl^- concentration is close to the detection limit (Farah et al., 2021; Freney et al., 2011) and is therefore not considered in the present study. The equivalent black carbon (eBC) concentrations are obtained from MAAP. These mass concentrations are used to calculate the aerosol refractive index which is further used in the determination of the lidar ratio, as explained in detail in the Section 3.

2.2. CALIOP instrument

The spaceborne lidar CALIOP (Cloud-Aerosol Lidar with Orthogonal Polarization) onboard the CALIPSO (Cloud-Aerosol Lidar and Infrared Pathfinder Satellite Observations) satellite provides a global dataset of the vertical structure of the entire atmosphere since 2006 (Winker et al., 2010) and is largely used in the atmospheric community. It allows to derive an estimate of the Lidar Ratio at the global scale from the aerosol type identification algorithm (Omar et al., 2009; Kim et al., 2018). In the present study, we use the CALIOP aerosol layer product (version 4.2) called Initial_532_Lidar_Ratio at 5 km horizontal resolution using the 532 nm signal. This product is based on the CALIOP version 4 (V4) algorithm which assumes a constant LR value for each aerosol layer that depends on the dominant aerosol type (Kim et al., 2013). The classification algorithm uses altitude, location, surface type, particle depolarization ratio and integrated attenuated backscatter to identify the different types of aerosols (Omar et al., 2009). Lidar ratios for the different aerosol types considered in the CALIOP classification algorithm are inferred from airborne HSRL (High Spectral Resolution Lidar) observations (Burton et al., 2013; Groß et al., 2013) or from ground based Raman lidar network (Müller et al., 2007; Tesche et al., 2009). The V4 algorithm was improved compared to previous versions, including the

introduction of a new aerosol subtype (dusty marine) and modified definitions of polluted continental and smoke aerosols. The aerosol types classified by CALIOP are 'polluted continental', 'polluted dust', 'clean continental' and 'dust' with lidar ratios of 70 ± 25 sr, 55 ± 22 sr, 53 ± 24 sr and 44 ± 9 sr, respectively. The classes 'clean marine' and 'dusty marine' in the CALIOP V4 algorithm are associated with the lower lidar ratios: 23 ± 5 sr and 37 ± 15 sr, respectively (Kim et al., 2018). In addition to the Initial_532_Lidar_Ratio, a Final_532_Lidar_Ratio is provided in the data files. Compared to the first one which uses only the aerosol type to assign a lidar ratio, the second uses the extinction calculated from the layer optical depth when available otherwise, it gives the same. These two products have been used in this study but as the results are very similar, only the figures with the Initial_532_Lidar_Ratio product are shown (called Initial LR). Figures with the Final_532_Lidar_Ratio (called Final LR) are available in supplementary materials.

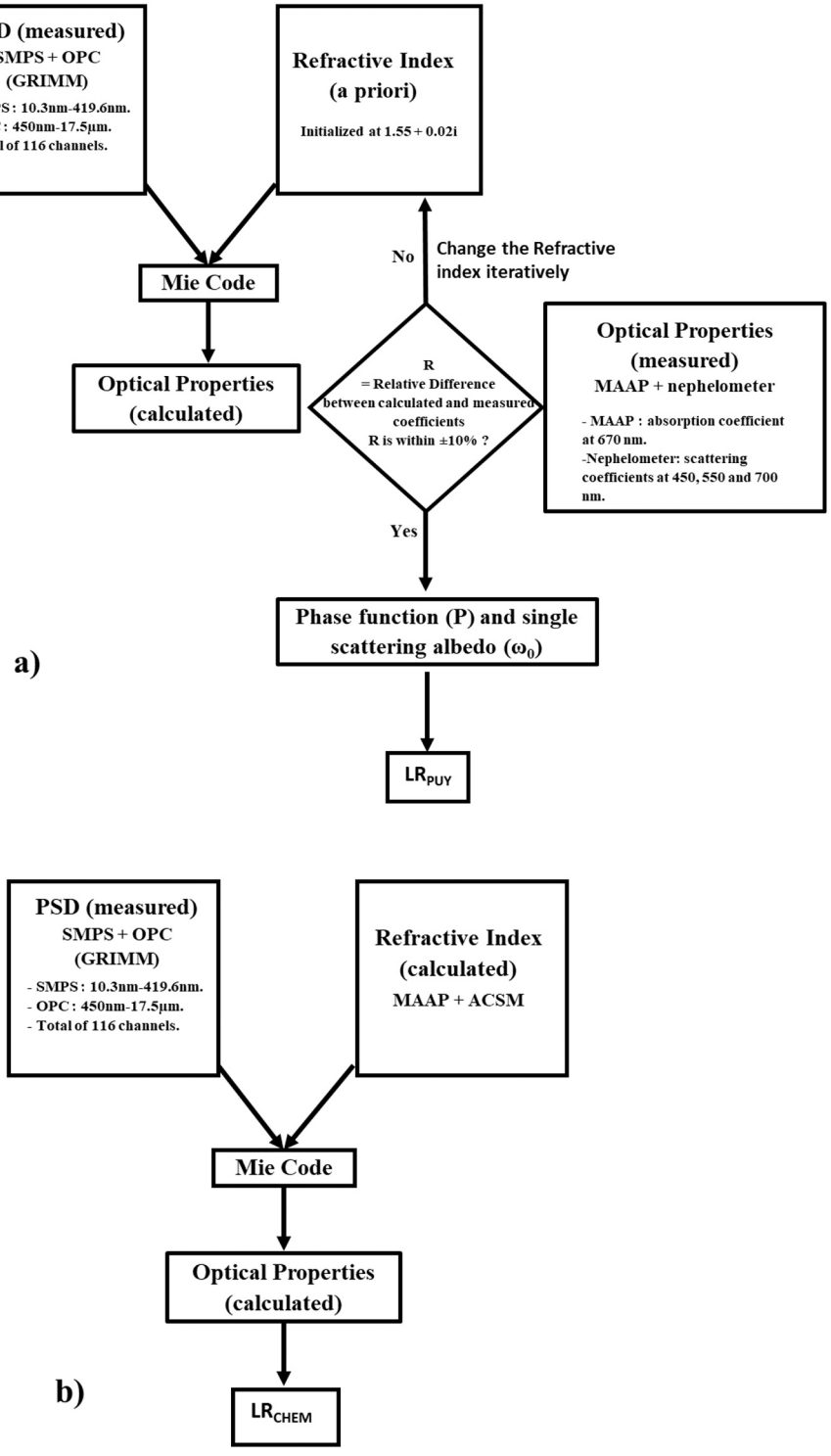

Fig. 1. Flowchart of the methodology of lidar ratio calculation using PUY station measurements of particle size distribution along with aerosol optical properties (LR_{PUY}) (a) and chemical composition (LR_{CHEM}) (b), respectively.

3. Methodology

The data used in this study were acquired in 2015 and 2016 when all the instruments worked.

3.1. Calculation of LR under dry conditions using optical measurements

Fig. 1a shows the flowchart of the entire methodology to produce LR_{PUY} derived from optical properties measured at PUY. The lidar ratio is calculated at 532 nm to be compared at lidar measurements performed at this wavelength by the CALIOP space-borne lidar. The optical parameters are thus calculated at 532 nm at hourly resolution. All in situ measurements performed at the station are under dry conditions (relative humidity lower than 40% at the inlet). The absorption coefficients are calculated at 532 nm using an absorption angstrom exponent of 1 (Eq. (1)), assuming that the absorption is mainly driven by black carbon (Russell et al., 2010):

$$\sigma_a^{532} = \sigma_a^{670} \cdot \left(\frac{532}{670}\right)^{-\alpha_a} \quad (1)$$

where $\boldsymbol{\sigma_a^{532}}$ is the absorption coefficient calculated at 532 nm, $\boldsymbol{\sigma_a^{670}}$ is the absorption coefficient measured at 670 nm and $\boldsymbol{\alpha_a}$ is the absorption angstrom exponent.

The scattering coefficients are calculated at 532 using the scattering angstrom exponent (450–700 nm) calculated from nephelometer data following Eq. (2):

$$\sigma_s^{532} = \sigma_s^{450} \cdot \left(\frac{532}{450}\right)^{-\alpha_s^{450-700}} \quad (2)$$

where $\boldsymbol{\sigma_s^{532}}$ is the scattering coefficient calculated at 532 nm, $\boldsymbol{\sigma_s^{450}}$ is the scattering coefficient measured at 450 nm and $\boldsymbol{\alpha_s^{450-700}}$ is the scattering angstrom exponent between 450 nm and 700 nm.

We calculated the hourly lidar ratio (LR_{PUY}) at 532 nm using a Mie code assuming that the particles are spherical. A T-Matrix would be more appropriated for non-spherical particles if we can understand particle type, shape, and aspect ratio for each range of the particle size distribution. However, facilities at PUY do not allow such studies and, at this occasion, the Mie code corresponds to the solution using the fewest assumptions. The Mie code uses the particle size distribution (PSD) obtained from the SMPS and OPC along with an arbitrary initial refractive index (1.55 + 0.02i) as inputs. The code provides the aerosol optical properties as outputs, including scattering and absorption coefficients. The refractive index is changed iteratively until the absorption and scattering coefficients produced by the Mie code had <10% difference with those measured by the MAAP and nephelometer instruments, respectively. The single scattering albedo (SSA or ω_o) and the phase function at a scattering angle of 180° (P), both also obtained as an output of the Mie code, are finally used to calculate the LR_{PUY} according to Shin et al., 2018:

$$LR_{PUY} = \frac{4\pi}{\omega_o P(180°)} \quad (3)$$

In the calculation of LR_{PUY}, the totality of the aerosol population (sub and super-micron) is assumed to have the same chemical composition, which is generally not the case (Bourcier et al., 2012). Hence, the method provides a lidar ratio which is an average between the sub and super-micronic modes.

3.2. LR Comparison by using aerosol chemical composition

With the aim to investigate the link between LR and aerosol composition in coming years, LR have also been calculated by using the chemical composition of the submicron non-refractive aerosol obtained from the ACSM and MAAP under dry conditions. In addition, this allow to evaluate the coherence of the LR_{PUY} obtained with all the observations available at PUY. Regarding the lidar measurements conducted at PUY up to now, we only have a 355 nm backscatter lidar 11 km from the PUY station with a full overlap between the telescope and the laser at an altitude too high for now to allow to retrieve LR at the puy de Dôme altitude (1465 m.a.s.l). Fig. 1b shows the flowchart of the entire methodology to produce the LR_{CHEM} by using the chemical composition. For this method, using particle chemical and mass concentration derived from the ToF-ACSM, the refractive index of the sampled aerosol population m is calculated using the particle volume concentration V_i and their corresponding refractive indices m_i taken at 550 nm from the literature (Highwood et al., 2012, 7262 Table 5): 1.53 for $(NH_4)_2SO_4$; 1.538–0.02i for organic carbon (OC); 1.95–0.79i for black carbon (BC) and 1.611 for NH_4NO_3 according to Chýlek et al., 1988:

$$m = \sum_i V_i . m_i \quad (4)$$

Using the refractive index of the aerosol mixture, LR_{CHEM} is obtained using the same procedure as LR_{PUY} without the repeated iteration (Fig. 1b). Fig. 2a shows the comparison between the hourly LR_{CHEM} and LR_{PUY} for different OC to eBC (equivalent Black Carbon) concentration ratios. Only clear-sky days, when both values of LR_{CHEM} and LR_{PUY} were available, have been used. This corresponds to 259 hourly data points.

A good correlation between the two data sets is obtained ($R^2 = 0.45$), although LR_{CHEM} presents higher values than LR_{PUY} (Fig. 2a). The difference could be due to several factors. In particular, the scattering properties of each chemical species used in the calculation were taken from the literature, with a large uncertainty on the scattering of some species, in particular organic species that account for more than half of the submicron particle mass (Farah et al., 2021). Lastly, super-micron aerosols were neglected in the calculation of LR_{CHEM}. However, the fact that the correlation between LR_{PUY} and LR_{CHEM} is good illustrates that the difference between the two calculation methods is not air mass type dependent. If the discrepancy between LR_{PUY} and LR_{CHEM} was due to the presence of super-micron particles then this would lead to a non-uniform ratio between both. The constant ratio between LR_{PUY} and LR_{CHEM} likely indicates a constant error in the refractive index of organic aerosols. The bias was high for low OC to eBC ratio. The refractive index of the aerosol mixture initially was calculated assuming the refractive index of eBC to be the same as that of pure black carbon. However numerical studies have shown that coated black carbon aerosols have lower imaginary part than pure black carbon (Zhang et al., 2019, 2020). We modified the refractive index of OC and eBC by reducing their imaginary parts. It is seen from Fig. 2b that the bias is reduced when the imaginary part is one fourth the initial values used in Fig. 2a. The results seem to indicate that the carbon particles measured by the MAAP are coated or mixed with other particles (Feng et al., 2021; Mallet et al., 2004). The resulting OC refractive index was closer to the refractive index of particulate organic matter in dry state at 550 nm (von Hoyningen-Huene et al., 1999), as may be the case above the boundary layer in a less humid environment. We will focus only on LR_{PUY} for the rest of this work to study the variability of the LR observed at PUY according to the air mass trajectories as more data is available.

3.3. Effect of humidity on LR calculation

To be compared to lidar measurements available in the literature, LR have to be calculated in atmospheric conditions and not in “dry” conditions as it is the case due to the sampling method. Thus, the Hygroscopic Growth Factor (HGF) is used to modify LR_{PUY} to calculate a LR in real atmospheric conditions called LR_{PUYwet}. The HGF has been parameterized based on the relative humidity, season and air mass origin observed at PUY during two years by Holmgren et al. (2014). The parameterization is as follows:

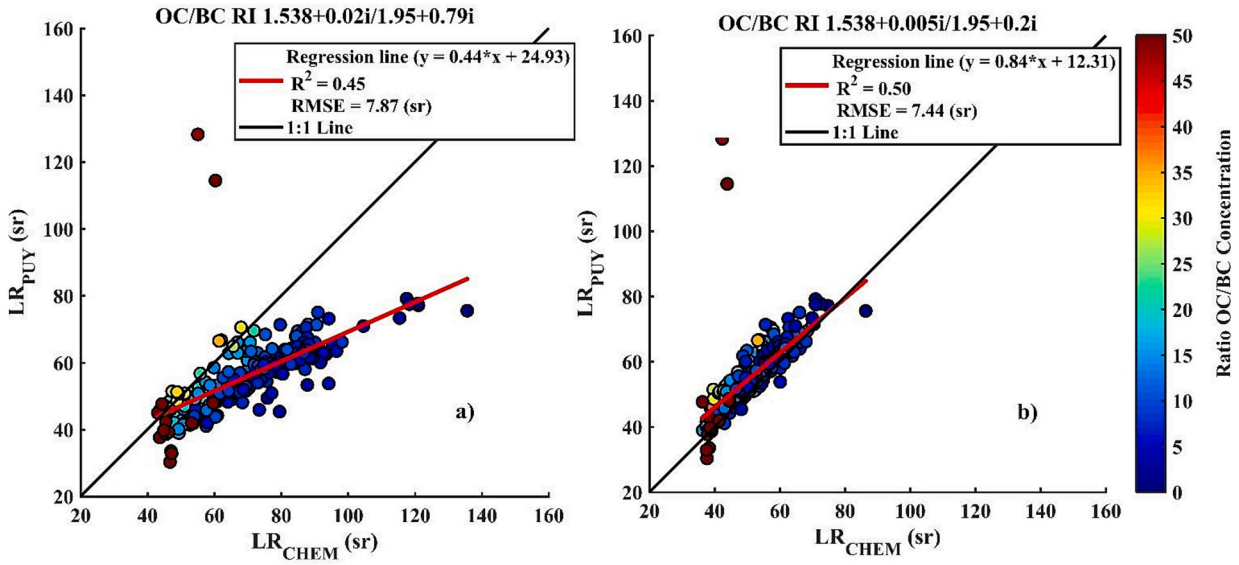

Fig. 2. a) Comparison between hourly lidar ratios obtained by the chemistry method (LR_{CHEM}) and using the optical instruments (LR_{PUY}). Both the LR are calculated under dry conditions. b) LR_{CHEM} vs. LR_{PUY} after reducing the imaginary part of the refractive indices of Organic Carbon (OC) and equivalent Black Carbon (eBC). The colorbar represents the ratio of OC to eBC concentrations.

$$HGF = \left(1 - \frac{RH}{100}\right)^{\gamma} \tag{5}$$

with

$$\gamma = -a\left(\frac{dp}{1\ nm}\right) - b \tag{6}$$

Where RH is the relative humidity measured in percent and dp is the particle diameter in nanometers. The a and b parameters depend on the season and air mass origin and are taken from Holmgren et al. (2014).

The wet refractive index m_{wet} is obtained using the volume weighted mixing rule detailed in Flores et al. (2012) at a mean dry diameter of 110 nm and with the refractive index of water, 1.33 + 0i:

$$m_{wet} = \frac{\left(\left(110^3.m_{dry}\right) + \left(\left((110.HGF)^3 - 110^3\right)1.33\right)\right)}{(110.HGF)^3} \tag{7}$$

where m_{dry} is the refractive index obtained after iteration in the calculation of LR_{PUY} using Eq. (3). The HGF from Eq. (5) is used to calculate the wet PSD from the dry PSD. Both the wet concentrations and the wet refractive index m_{wet} are then used as input to the Mie code to calculate the new LR_{PUY} using the Eq. (3) referred as LR_{PUYwet} throughout the paper. The HGF parameterization is not well adapted for particle diameters beyond 420 nm and is overestimated for relative humidity >90% (Rose et al., 2013). Therefore, for the current study, the effect of humidity is studied only for cases when the relative humidity is <90% and the HGF at 420 nm is applied for particles having diameters larger than 420 nm.

For the analysis of LR at PUY, we only consider days when all measurements were done under clear skies. We exclude cases when the site was in-cloud conditions which is encountered 60% of time in winter and 24% in summer in average (Baray et al., 2019), and hence consider

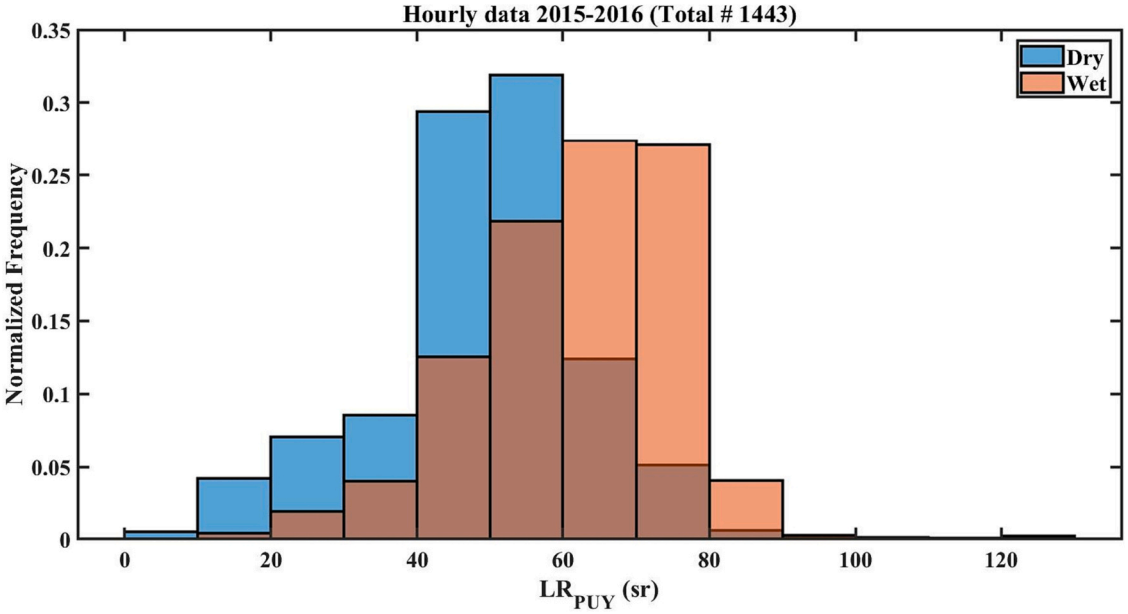

Fig. 3. Histogram of hourly LR_{PUY} values for 2015–2016 in dry (blue) and wet (red) conditions.

only cases when the relative humidity was <90%, and the liquid water content was <0.4 g m^{-3}, and no frost was present (Hervo et al., 2014). Fig. 3 shows two histograms of the LR_{PUY} distribution, one in dry condition and the other in wet condition over the period 2015–2016. On this figure, we can see LR_{PUY} increases due to humidification as the refractive index decreases closer to that of liquid water and the PSD shifts towards larger diameters (Ferrare et al., 2001) similar to the continental model proposed by Ackermann (1998). This increase between LR_{PUY} dry and wet is about 10–15 sr (average values are LR_{PUYdry} = 49 sr and LR_{PUYwet} = 62 sr). Hourly LR_{PUYwet} have a wide range of values with >50% of the total 1443 hourly values between 60 sr and 80 sr and few values above 80 sr.

All high LR_{PUYwet} values (>100 sr) are observed and find associated with low single scattering albedo measured at the station (<0.75 at 532 nm). These high values are usually associated with spherical particles which are highly absorbing and have a narrow mono-modal distribution (Josset et al., 2011).

3.4. Air mass trajectories

To study the variations of LR_{PUYwet} observed at the PUY station, trajectories were performed in order to know the air mass history of the 1443 in situ hourly observations. Therefore, for every hour during 2015–2016, when conditions and all instruments were available for LR_{PUYwet} calculation, trajectories using the CAT model (Computing Atmospheric Trajectory Tool) (Baray et al., 2020) were calculated. The CAT model uses the wind field provided by ECMWF ERA-5 reanalysis (3 h temporal resolution and 0.25° spatial resolutions in latitude and longitude) as input and a 10 km resolution topography matrix (Bezděk and Sebera, 2013). For the present study, for each hour, 45 trajectories are calculated in a 0.2° domain around the PUY station using 5 vertical levels spaced out every 1 hPa and 9 release points spaced out every 0.1° at each altitude starting 50 m below the PUY station altitude to take into account the air masses that arrive below the summit and go up the slopes. The temporal resolution of the back-trajectories is 15 min and the total duration 96 h. This configuration is a good compromise between accuracy and computation time and is well adapted for synoptic studies.

4. Results

4.1. Analysis of LR based on sectors and comparison with literature

Many sectors (residential, industry, traffic, agriculture …) can impact the aerosol load of the geographical region around PUY. Since PUY is a mountain station, observations are also influenced by long-range transport aerosols when the station is in the free troposphere (Farah et al., 2018). Similar to previous work on the PUY site, the geographical sectors used to classify air masses sampled at PUY for the present work are - Africa, Atlantic, Marine Modified, Europe and Local (Hervo et al., 2014; Bourcier et al., 2012). These sectors are presented on Figs. 5 and 6. The air masses in the Africa sector are usually a mixture of dust from the Sahara, marine aerosols from the Mediterranean Sea and polluted aerosols from the Mediterranean basin. The Atlantic sector consists of mainly marine type aerosols which might also be influenced by long-range transport aerosols from Canada/North America. The Marine Modified sector is a small sector which contains oceanic air masses influenced by the Northern European regions, mainly influenced by the North of Germany, Denmark, but also including Great Britain, Ireland and Scandinavia. They are a mixture of marine and anthropogenic aerosols (Sellegri et al., 2003). Continental aerosols, including biomass burning, traffic and industrial pollution, are found in the Eastern European sector. The Local sector is a 2° radius circle around the PUY station. It is considered to be mainly influenced by local aerosols i.e., by aerosols that are transported from nearby sources.

Fig. 4 shows the boxplots of LR_{PUYwet} for the different geographical sectors. The statistics for one sector are calculated using all the trajectories crossing this sector. A trajectory can thus account for several sectors. The LR_{PUYwet} associated to one trajectory is repeated in the calculation of the mean LR of a sector according to the number of points of the given trajectory present in that sector. The mean LR of a sector is in fact a weighted LR average where the weights are the number of trajectory points (i.e. time spend) in that sector considering that more time an air mass stay in a sector, more the air mass is influenced by the environment of that sector and thus could be representative of this sector. Among the 1443 × 45 trajectories calculated, 40% of the points were located in the Africa sector, 25.7% in the Atlantic sector, 8.1% in the Marine Modified sector, 23.5% in the Europe sector, and 2.7% in the Local sector.

When we compare quartiles, higher LR values are observed at PUY when air masses crossed European sector and lower LR values are observed at PUY when air masses crossed Atlantic or Marine Modified sectors. In addition, the distribution is quite-symmetric for Atlantic and Marine Modified sectors and left-skewed for Europe and Local sectors. In the following subsections, we compare the values obtained with those available in the literature.

- Africa sector

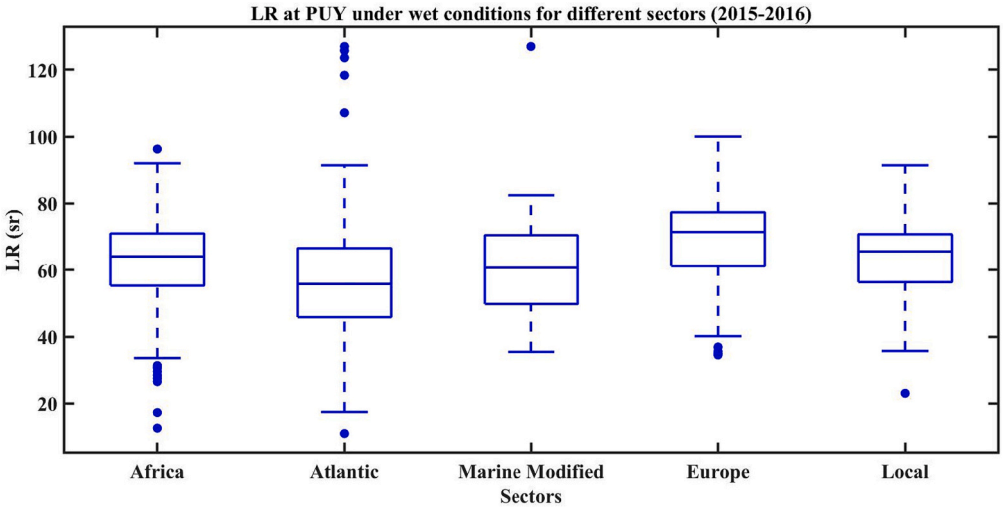

Fig. 4. Boxplots of LR_{PUYwet} at 532 nm for different geographical sectors. On each box, the central line indicates the median, and the bottom and the top indicate the 25th and 75th percentiles, respectively. Beyond the whiskers, data are considered as outliers and are represented by circle markers.

The mean and standard deviation LR_{PUYwet} for air masses from the Africa sector are 63 ± 11 sr at 532 nm. Since the Africa sector consists of North Africa, the Mediterranean basin and a part of the Atlantic Ocean, air masses are heavily influenced by pure dust or a mixture of dust, marine aerosols and pollution (Berjon et al., 2019; Ancellet et al., 2016; Mona et al., 2006). Navas-Guzmán et al. (2013) analyzed the aerosol properties over southeastern Spain using Raman lidar measurements at 532 nm from 2008 to 2010. They found that average LR during spring and summer was ~46 sr with a large standard deviation (SD) associated with the presence of mineral dust aerosols. Kim et al. (2020) found the lidar ratio for Saharan dust to be 49.5 ± 36.8 sr (532 nm). They also reported the lidar ratios for dust aerosols transported to the Mediterranean Sea (44.4 ± 15.9 sr) and Mid Atlantic (40.3 ± 12.4 sr). Fresh Saharan dust and mixed Saharan dust are about 48 ± 5 sr and 50 ± 4 sr (at 532 nm), respectively according Groß et al. (2013) work. The eastern Mediterranean area is also influenced by biomass burning aerosols from Eastern Europe, maritime aerosols (both local and from the west), and local pollution. The major contribution of aerosols in the central Mediterranean basin are those from continental Europe with a LR of 72 ± 20 sr (at 440 nm). Other aerosol types, including dust aerosols and marine aerosols (polluted and clean), are also present having a LR of 43 ± 15 sr and 58 ± 24 sr, respectively (Santese et al., 2008).

The mean LR_{PUYwet} is higher than previous studies mentioned above. However, dust influenced LR values also depend on the location, type of mixture and the percentage of dust present (Groß et al., 2013, 2495–2499, Table 3–5). LR_{PUYwet} agrees well with long-range transported dust (~59 sr) (Groß et al., 2013). The mixing process and the transport time also result in the variation in the LR of dust aerosols (from 42 sr to 79 sr at 532 nm) (Soupiona et al., 2019). LR_{PUYwet} agrees well with Raman lidar measurements at Munich (59 sr at 532 nm) which were similar to SAMUM (Saharan Mineral Dust Experiment) campaigns implying no change in the optical properties of Saharan dust for transport time less than a week (Wiegner et al., 2011).

- Atlantic and Marine modified sectors

The air masses from both the Atlantic and Marine Modified sectors contain usually a mixture of marine aerosols and pollution from nearby land masses. The PUY station, being a mountain site, is not under marine conditions. However, measurements at the station have detected air masses which have travelled above the ocean keeping some characteristics of the source signature even after possible aging (Farah et al., 2018, 2021). As westerlies winds are dominant in France and the PUY site is around 350 km eastward from the Atlantic Coast, air masses from these sectors are observed 36% of the time based on >4 years of data (Holmgren et al., 2014). The mean and standard deviation LR_{PUYwet} for the Atlantic and Marine Modified sectors are ~56 ± 16 sr and 60 ± 13 sr, respectively. Dust sources present in high-latitudes result in a higher LR near the coast of Iceland and contribute to pollution over the nearby oceans (Dagsson-Waldhauserova et al., 2017; Prospero et al., 2012). The coastal area of Dunkerque (France), close to the North Sea had a mean aerosol LR of 33 ± 14 sr at 355 nm during the sea breeze (Boyouk et al., 2011). McAuliffe and Ruth (2013) reported the LR over southern Ireland to be 20–25 sr (at 532 nm) typical for marine conditions, with occasional dust events mixed with local pollution resulting in an increase in the LR to 40–50 sr. Therefore, higher LR_{PUYwet} values encountered for the Atlantic and Marine Modified sectors can be explained by such occasional pollution or by aerosol aging before reaching the PUY station.

- Continental sector

Aerosol sources over land consist of a mixture of both natural and anthropogenic sources from both local regions and those transported over long distances. At a central European site, local and anthropogenic haze observed by Raman lidars, resulted in a mean LR of 53 ± 11 sr (Müller et al., 2007). A study from 2008 to 2018 using lidar and neural networks classified the different aerosol types across Europe (Nicolae et al., 2019). The typical type of aerosol particle was medium-sized, medium absorbing with low spectral dependence. Smoke was the dominant aerosol type in Eastern Europe, whereas, continental aerosols dominated central and northwestern Europe. The mean LR across the entire Europe at 532 nm was 67 ± 4 sr. Janicka and Stachlewska (2019) analyzed the observations of aerosol mixtures at Warsaw from August 9th to 11th 2015 using a multiwavelength Raman-polarization and water vapor lidar. The aerosol mixture, when dominated with fresh or aged (2–3 days) biomass burning aerosols, had LR ranging from 57 sr to 85 sr at 532 nm. The LR_{PUYwet} for the Europe sector, 68 ± 12 sr, are in agreement with these values.

- Local sector

The mean of the Local sector has been calculated with all the 1443 LR_{PUYwet} but with a weight in the average calculation for each depending of the time their associated trajectories stay in that sector. The Local sector has LR values, 62 ± 13 sr, similar to the values of the Africa sector since this sector represents around 40% of all the trajectories points. Indeed, these backward trajectories crossing the Africa sector, starting at PUY, are accounted in the Local sector for all trajectory points remaining within 2° of PUY. Even if some trajectories stay more long time in the Local sector than others, it does not change a lot this percentage.

4.2. Analysis of LR based on air mass history

The analysis is refined by calculating LR_{PUYwet} mean using grid cells of 2° x 2° instead of sectors (Fig. 5a). As for sectors, the LR shown are not those observed at the location of the grid cell but those observed at the PUY station. The mean LR in a grid cell is calculated using LR values at PUY when the trajectories cross the corresponding grid cell. The number of LR observations at PUY, used to calculate the mean is given on Fig. 5b. Only bins with >10 values are reported for significance. Fig. 5a shows the mean LR_{PUYwet} in each grid cell. Outside the box [50°W/30°E, 35°N/65°N] around PUY, LR values are less robust due to the lower number of trajectory points present in these grid cells (dark blue points on Fig. 5b). Overall, LR values correspond to expected aerosol types (see previous sub-section).

LR calculated at PUY are above 60 sr when air masses come from the Eastern Europe (Fig. 5a). These mean values are consistent with values reported in Europe for smoke and haze and could be representative of a mixture of such situations. For examples, using Raman lidar, Alados-Arboledas et al. (2011) observed at Granada in Spain, LR of 60–65 sr for quite fresh smoke. Haarig et al. (2018) have observed in Leipzig (Germany) high LR at 532 nm between 65 and 80 sr for August 2017 Canadian fires. High values are also reported in the literature for polluted continental air masses. For examples, Chazette and Royer (2017) derived from ground-based sun photometer measurements, LR between 67 and 77 sr in Paris area, France and Müller et al. (2007) show also that the highest lidar ratios with values close to 70–80 sr were observed at Hamburg and Leipzig in cases where air masses were advected from east Europe which correspond to meteorological situations considered to build the map shown in Fig. 5a. For the values close to or above 80 sr located between 52°N and 60°N and with longitudes higher than 30°E, they are at the border of the domain and thus the means in each pixel is calculated with less values. Only 53 different LR hourly values were available in this area recorded during 8 different days: 10/02/2015; 10/15/2015; 11/02/2015; 11/03/2015; 10/07/2016; 10/08/2016; 10/09/2016 and 10/11/2016 all during the autumn season. These values are thus linked to specific air mass transport and cannot be considered as representative of the annual average at this location.

LR calculated at PUY are lower, between 40 and 60 sr when air masses come from the Atlantic Ocean. The values in the Atlantic sector appears to be variable and larger on average than expected for marine

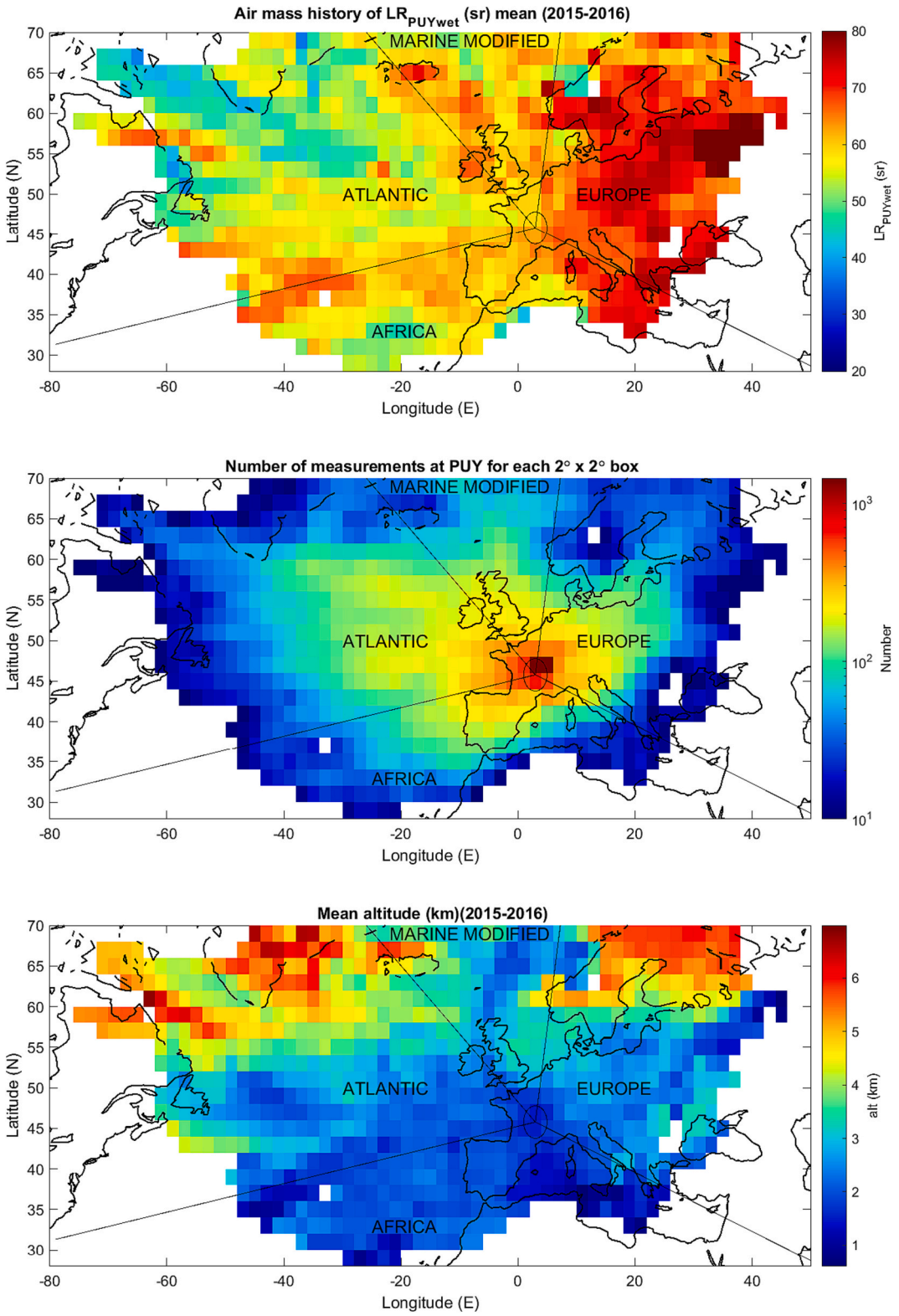

Fig. 5. a) Mean LR_{PUYwet} derived from backtrajectories in 2° x 2° grid cells b) Number of values LR_{PUYwet} used to calculate the means and c) Mean altitudes of the trajectories in 2° x 2° grid cells.

aerosols. This is further discussed. It is found that LR calculated at PUY are higher when the air mass crosses continents than when it comes from the surrounding oceans only. This is true for Greenland, Iceland and Ireland. However, for countries close to inland seas, we get similar LR means when air mass cross countries or seas as for Sweden and Baltic sea, Greece and Mediterranean Sea, Bulgaria, Romania, Ukraine and Black Sea.

According to Tomasi et al. (2015), aerosol measurements over the oceans around Northern Scandinavia indicated that during spring, the atmospheric column consists of anthropogenic and natural sea-salt aerosols. They reported the annual LR to be within 30–50 sr (532 nm) measured at Ny-Ålesund station. A paper based on EARLINET (European

Aerosol Research Lidar Network) stations has also shown with HYSPLIT trajectories that aerosols with marine signature are observed on Kuopio, Finland or Potenza, Italy and have lower LR than other air mass origins (Mylonaki et al., 2021, Table 4).

Fig. 5c shows the mean altitude of the trajectories in each grid cell. For the Atlantic and European sectors, airs masses from Scandinavia and Greenland come from higher mean altitudes (> 5 km) compared to the rest of the sectors. The large variability in the LR over the ocean can be due to the presence of long-range transport aerosols. Vaughan et al. (2018) observed the transport of Canadian forest fire smoke across the Atlantic Ocean over the United Kingdom during May 2016. Using Raman lidars, they reported LR in the range 35–65 sr at 355 nm. However the variability in altitude observed in our study does not seem to explain all the variability of the LR observed in each sector on Fig. 5a. The Africa sector is the sector where the mean altitudes are the lower (below 2 km height).

4.3. Indirect comparison with CALIOP measurements

CALIOP provide LR at 5 km resolution in all the area studied allowing to compare the spatial distribution. According to the flowchart of the aerosol subtype selection scheme (Fig. 1 from Kim et al., 2018), aerosols are discriminated according to the altitude of the layer. Above ocean, a layer with an estimated particulate depolarization ratio between 0.075 and 0.2 could be classify as dusty marine or polluted dust depending if the base of the aerosol layer is below or above 2.5 km respectively. Always above ocean, for estimated particulate depolarization ratio below 0.075, aerosols could be classify as marine (or polluted continental/smoke in case of very low particulate depolarization ratio) or elevated smoke depending if the top of the aerosol layer is below or above 2.5 km respectively.

For the two cases (base of the aerosols layers below or above 2.5 km), for each grid cell, the aerosols layers detected by CALIOP are used to calculate a mean LR. Fig. 6 shows the spatial distribution of the mean Initial LR assigned by CALIOP (LR_{CALIOP}) for all overpasses (and not only those intersecting backtrajectories from PUY when measurement have been done there) passing through every 2°x2° grid in the 80 W-50E and 20 N–70 N domain for the 2015–2016 time period. It must be underlined that the LR maps of CALIOP (Fig. 6) cannot be directly compared to the LR map built from PUY observations (Fig. 5a). Indeed, it is possible that CALIOP detects some aerosols layers corresponding to air mass types which are never observed at PUY because they are never advected above Western Europe. In addition, aerosols can be transformed during their transport by aging and mixing that is not taking into account on the LR map of PUY. One exception is the local sector for altitudes below 2.5 km which includes the PUY station as PUY measurements performed at the station have been slightly advected and could be statistically directly compared to CALIOP measurements. For this sector (see also previous subsection), LR_{PUYwet} (62 ± 14 sr) are in good agreement compared to LR_{CALIOP} (61 ± 11 sr for initial lidar ratios and 58 ± 15 sr for final lidar ratios) showing quite the same mean and variability.

For the other sectors, the statistical comparison between Figs. 6 and 5 must be carefully discussed to check how relevant the LR spatial distribution derived from LR_{PUYwet} is.

For altitudes below 2.5 km, a strong contrast is observed above the ocean compared to the continent even for inland seas with much larger LR values above continents than above oceans. The CALIOP Initial LR over the coastal regions are intermediate between low LR values over open oceans and higher values over the continents (Burton et al., 2012). There is a possible "mistyping" of aerosol layers in these areas, due to

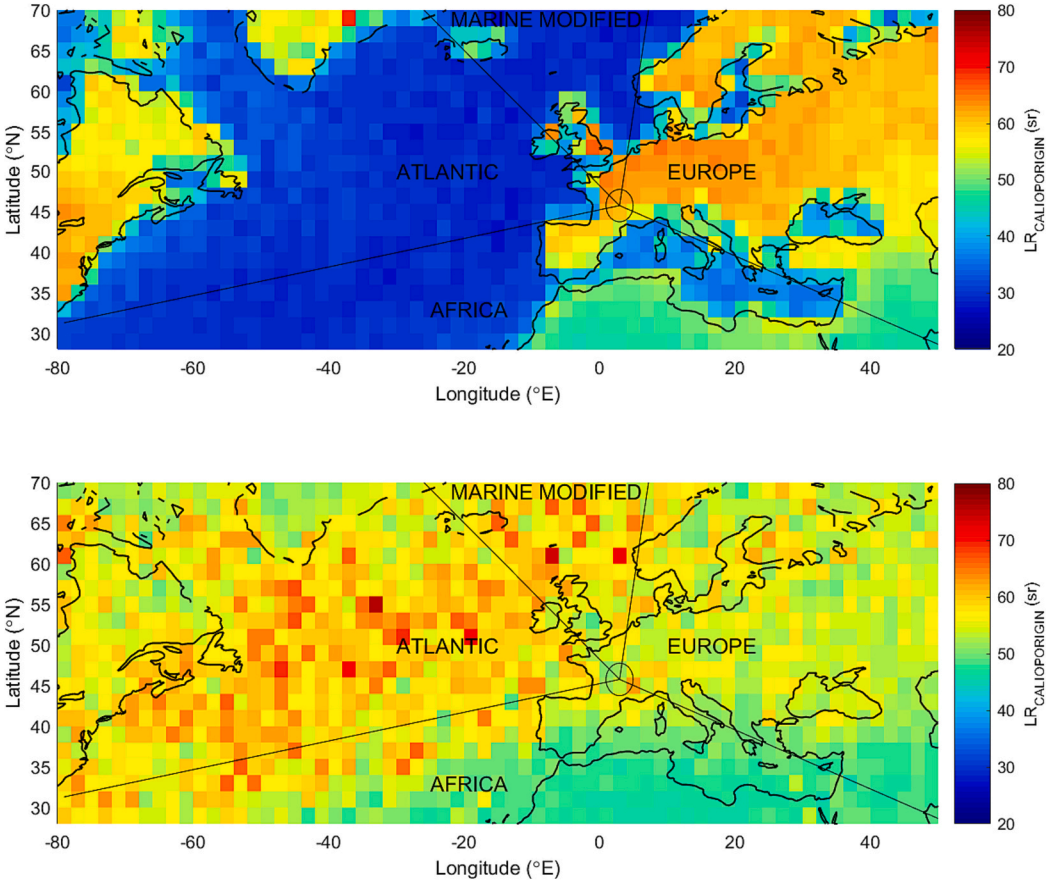

Fig. 6. Mean Initial LR_{CALIOP} calculated in 2°x2° grid box for the period 2015–2016 a) for aerosol layers bottoms below 2.5 km altitude and b) for aerosol layers bottoms above 2.5 km altitude.

mixing of marine aerosols with the outflow of continental pollution or dust, leading to errors in the retrieval of optical properties (Schuster et al., 2012). The ocean/continental contrast also exists when using the PUY data (Fig. 5) but with higher LR. Above the ocean, a majority of clean marine (LR = 23 sr) and dusty marine aerosols (LR = 37 sr) are observed by CALIOP explaining the smaller Initial LR values. Above continents, higher LR means are observed by CALIOP in Western Europe (France, Germany) and in USA compared to Eastern Europe and Canada. The lower LR means are observed for northern Africa and Turkey.

For the altitudes above 2.5 km, the contrast is reduced between oceans and continents in Fig. 6b with LR values being higher above ocean than above continents. The difference between the two altitudes ranges is more pronounced for Europe than the other continents with the presence of clean continental air masses ($LR_{CALIOP} = 53 \pm 14$ sr) instead of polluted continental air masses ($LR_{CALIOP} = 70 \pm 25$ sr) at lower altitudes. Above oceans, the high LR values are due to the large number of elevated smoke ($LR_{CALIOP} = 70 \pm 16$ sr) or polluted dust ($LR_{CALIOP} = 55 \pm 22$ sr) detected by CALIOP in this altitude range.

PUY and CALIOP show differences in patterns in the LR spatial distribution between ocean and continent or between low and elevated altitude range. It is difficult to know from statistical comparison if the difference is due to aerosols properties modification during transport by aging and mixing or if CALIOP performed observations of air masses never advected at PUY. To further analyze these differences, coincidences between CALIOP observations and backtrajectory positions performed from PUY observations have been selected using air masses observed first by CALIOP and after at PUY with the in situ instruments. We take a maximal temporal difference of 30 min and a maximal distance of 50 km between CALIOP observations and trajectories locations, because the mean distance (and standard deviation) travelled by the air masses, estimated with all the trajectories, is 32 ± 21 km in 30 min. The altitude of the trajectory must be within the altitude range of the CALIOP aerosol layer. Only 526 of the 1443 LR_{PUYwet} have such coincidences with CALIOP. As for one PUY measurement, we can have several CALIOP coincidences at different times along the trajectories, overall 901 coincidences are available when using the CALIOP Initial LR product and 916 coincidences when using the CALIOP Final LR product. Fig. 7 shows the density plots of the LR for coincidences in each sector. For each CALIOP LR values, the median of the coincident LR_{PUYwet} has been calculated and shown by an open circle on Fig. 7 (in black when there is <10 LR and in red when there is >10 LR to see the robustness). For the local sector, the agreement between CALIOP and PUY LRs is good with around 42% of the coincidences being "polluted dust" aerosol type and around 44% polluted continental or elevated smoke aerosol type. For the

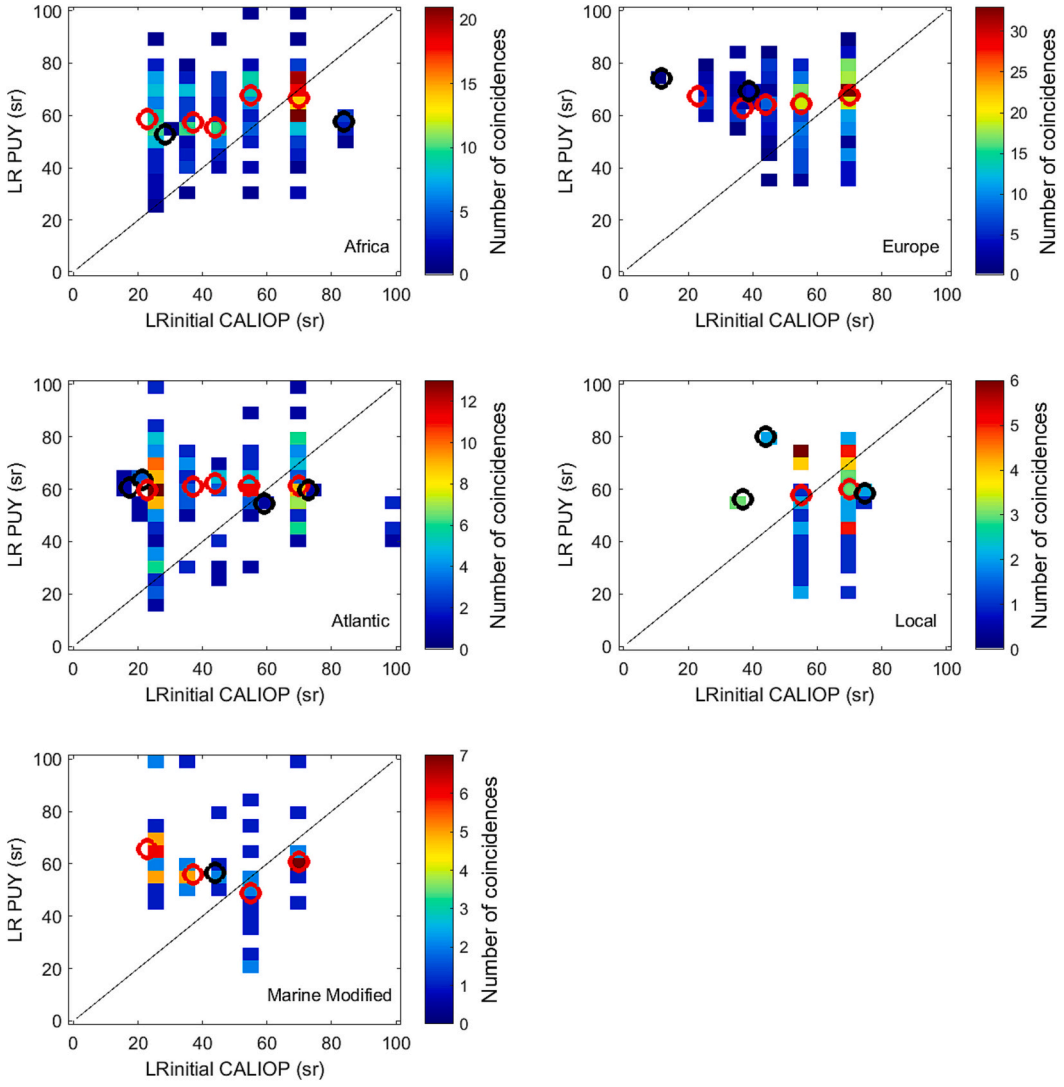

Fig. 7. Density plot of the LR for the coincidences founded between CALIOP (x-axis) and the backtrajectories calculated from PUY observations (y-axis) by bins of 5 sr for each sector indicated on the graph. For each CALIOP discrete value, the median of the LR_{PUY} has been calculated and shown by a circle in black when there is <10 LR and in red when there is >10 LR.

other sectors, and more particularly the Atlantic sector, two modes are evidenced, one at 55–70 sr and the other at 23 sr. The first one is in good agreement with advected LR_{PUYwet}. The second one at 23 sr is not observed at PUY where LR are higher even when these lidar ratios initially correspond to "clean marine" aerosol type identified by CALIOP in the Atlantic and Marine modified sectors. As such a difference between CALIOP and PUY LR is still observed when using coincident observations, they cannot be due to CALIOP observations of air masses never advected at PUY station. An error of attribution by CALIOP is still possible as discussed before, but modification of aerosol properties is another possibility. The same observations are made with the Final LR CALIOP; the only difference is the occurrence of LR lower than 20 sr retrieved in all sectors except the Local sector (Figure Annexe A.2).

To test this hypothesis, the sensitivity of the differences observed between Initial LR CALIOP and advected LR PUY to the transport parameters was thus investigated considering the distances and times spend between the coincidences and the PUY measurements as well as the layer altitudes. These results are show on Fig. 8 where the different colors correspond to the different CALIOP Initial LR values. For the 901 coincidences, CALIOP Initial LR are distributed as follow: ~35% of 70 sr (polluted continental/smoke/elevated smoke), ~20% of 23 sr (clean marine), ~14% of 55 sr (polluted dust), ~10% of 44 sr (desert dust), ~10% of 37 sr (dusty marine) and 7% of 53 sr (clean continental). Among these 901 coincidences, 72% have travelled >50 h between the CALIOP observation and the PUY station, 78% have travelled <1500 km between the CALIOP observation and the PUY station and 88% are layers below an altitude of 2.5 km. During 50 h, aerosols properties can evolve due to mixing and aging. Nevertheless, a good agreement is observed between CALIOP and PUY for CALIOP Initial LR of 70 sr, 55 sr and 53 sr not depending on the time and distance between both observations and on the altitude of the aerosols layers. For the lower CALIOP Initial LR, PUY provides higher values, on average. It is more pronounced for CALIOP Initial LR of 23 sr. However these aerosols of low altitude (< 2.5 km) have travelled at least 330 km and 9 h before being sampled by the PUY station and could have experienced an increase of LR during transport due probably to mixing with continental air or aerosol aging before reaching the station. The change in LR during transport depends on the change in the size distribution and the chemical composition, but also on aerosol sources crossed on the transport pathways taken by air masses before reaching the measurement site (Veselovskii et al., 2020; Müller et al., 2007).

5. Conclusion

In situ aerosol size distribution and optical measurements performed at the PUY mountain site have been used as inputs of a Mie code to calculate the 532 nm aerosol lidar ratio (LR) for the period 2015–2016. The LR obtained (LR_{PUY}) have been compared in dry conditions to LR calculated using the same Mie code but with a refractive index determined by the aerosol chemical composition (LR_{CHEM}) instead of the optical measurements. The two data sets show a good correlation. The overestimation observed in the LR_{CHEM} compared to the LR_{PUY} reduces

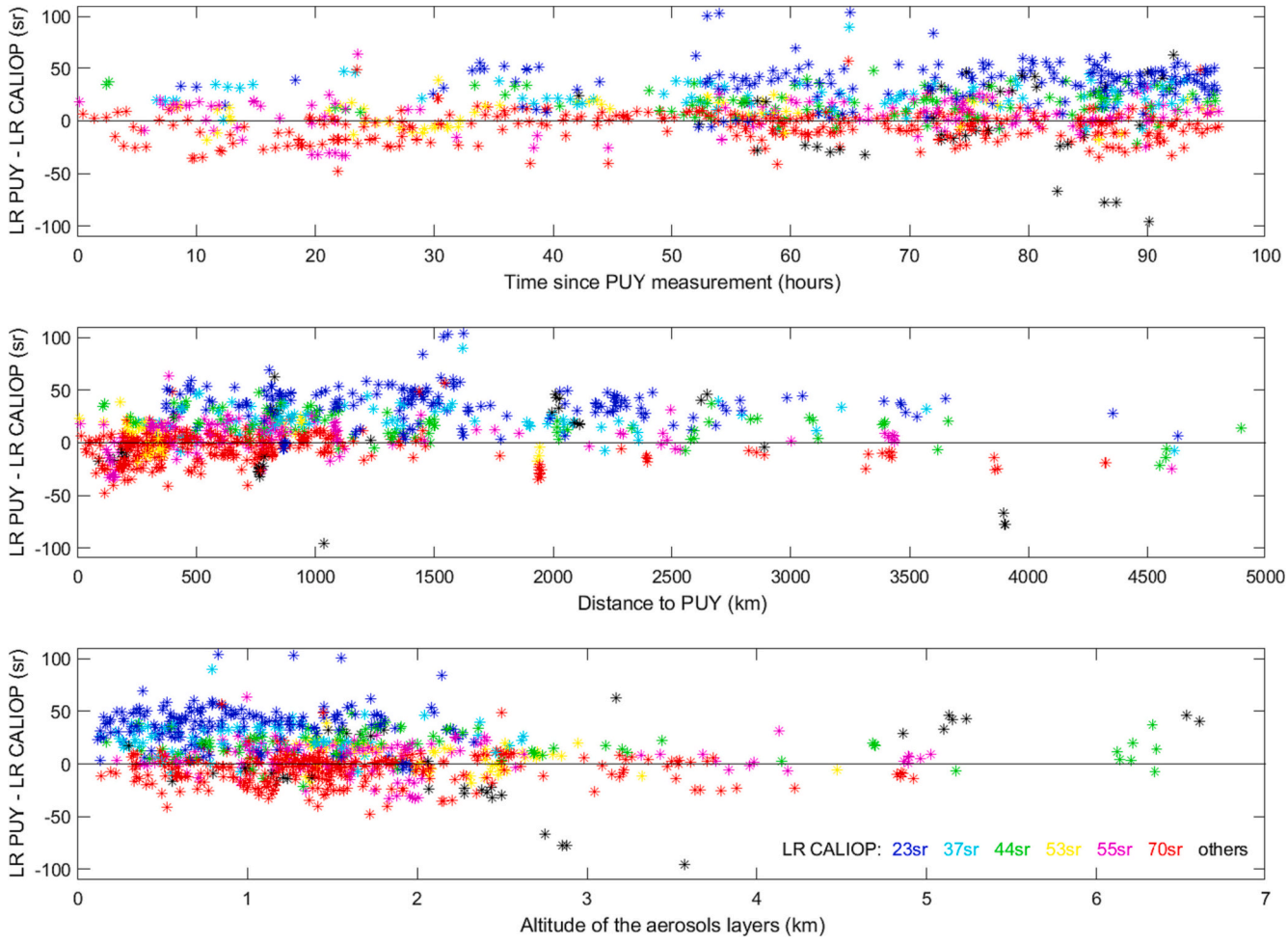

Fig. 8. Difference between LR_{PUYwet} and Initial LR_{CALIOP} for each coincidence depending on the time spend between the coincidences and the PUY measurements (top), the distance between the coincidences and the PUY station location (middle) and the altitude of the aerosols layers (bottom). The colors correspond to the different CALIOP Initial LR values existing (blue: 23 sr, cyan: 37 sr, green: 44 sr, yellow:53 sr, magenta: 55 sr, red:70 sr and black: other values).

when decreasing the imaginary part of the refractive index used for organic carbon and equivalent black carbon. The refractive index of the mixture initially was calculated assuming the refractive index of eBC to be the same as that of pure black carbon. However, the results suggest that the black carbon particles measured by the MAAP are mixed with other particles or coated.

Variability of the LR calculated at PUY from optical measurements was also studied according to air masses travel using backward trajectories. Statistically, lower LR are calculated at PUY for air masses transported from the Atlantic ocean compared to air masses having only travelled over continental surfaces in agreement with the literature (Kim et al., 2018; Burton et al., 2012; Müller et al., 2007). This ocean/land contrast is also observed by the spatial lidar CALIOP but with a more pronounced difference for aerosols layers below an altitude of 2.5 km. Inland seas have similar PUY advected mean LR to surrounding lands while it is not the case for CALIOP.

Over the same period (2015–2016), the LR calculated from PUY measurements (62 ± 14 sr) are in good agreement in terms of mean and variability with the CALIOP LR (61 ± 11 sr for the Initial LR product) for aerosols layers detected in a 2° radius circle around the PUY station at altitudes below 2.5 km. When using data with good spatial (<50 km) and temporal (<30 min) coincidences between CALIOP observations and backward trajectories performed from PUY at the time of the in situ measurements, the LR comparison shows two main results:

- For CALIOP Initial LR of 70 sr, 55 sr and 53 sr, a good agreement with advected PUY LR is observed with no dependence on the time and distance between both observations and on the altitude of the aerosols layers. This suggests few mixing during transport or mixing of similar air masses for continental, smoke and polluted dust aerosols types.
- For CALIOP Initial LR of 23 sr (clean marine aerosols), PUY LR are higher (~55–65 sr). A possible source of error may be due to the attribution of aerosol type in CALIOP algorithm. However, since these air masses, coming from the ocean, have crossed >300 km of land during at least 9 h at altitudes lower than 2.5 km before reaching the PUY station, they may have experienced mixing with continental air masses increasing their LR.

This paper is a preliminary study of a project aiming at combining the aerosols optical properties observed at global scale by satellite instruments, with the aerosol characterization (chemical composition and microphysical distribution) obtained from in situ observations at a mountain top station. For that, ACSM data is required to highlight a more robust relationship between LR and aerosol type deduced from the chemical composition. A deeper understanding of aerosol type, shape and aspect ratio would also improve in-situ methodologies. In addition, the new multiwavelength ground-based lidar COPLid which starts giving measurements end of 2022 on the Cézeaux site, approximatively 11 km east-south-eastward of the PUY station, will provide vertical distribution of the aerosol optical properties and will fill the gap between the calculations done with the in situ measurements of PUY and the global scale observations. It will also provide more information on the aerosol type thanks to the measure of the depolarisation at 355 nm and 532 nm.

Funding

K. E. salary was supported by the Centre National d'Etudes Spatiales (CNES, EECLAT project: https://eeclat.ipsl.fr/). Ground based aerosol data are financially supported by INSU and the SNO CLAP project and quality controlled in the frame of the ACTRIS research infrastructure. The CO-PDD instrumented site is managed by the OPGC observatory and LaMP laboratory, and funded by the Université Clermont Auvergne (UCA), by the Centre National de la Recherche Scientifique (CNRS-INSU), and by the Centre National d'Etudes Spatiales (CNES).

CRediT authorship contribution statement

Kruthika Eswaran: Methodology, Software, Validation, Formal analysis, Investigation, Writing – original draft. **Nadège Montoux:** Funding acquisition, Conceptualization, Supervision, Software, Investigation, Writing – review & editing. **Aurélien Chauvigné:** Conceptualization, Methodology, Software, Writing – review & editing. **Jean-Luc Baray:** Resources, Software, Writing – review & editing. **Gérard Ancellet:** Conceptualization, Resources, Writing – review & editing. **Karine Sellegri:** Conceptualization, Resources, Writing – review & editing. **Evelyn Freney:** Data curation, Writing – review & editing. **Clémence Rose:** Data curation, Writing – review & editing. **Jacques Pelon:** Resources, Writing – review & editing.

Declaration of Competing Interest

The authors declare that they have no known competing financial interests or personal relationships that could have appeared to influence the work reported in this paper.

Data availability

In situ data were extracted from the EBAS database (http://ebas.nilu.no/default.aspx; Tørseth et al. (2012)).

Acknowledgments

The CALIPSO/CALIOP data were obtained from the NASA Langley Atmospheric Science Data Center (https://subset.larc.nasa.gov/calipso/login.php). Acknowledgement is made for the use of ECMWF's computing and archive facilities in this research for trajectory analysis using the CAT model. The authors also thank the technical staff of the PUY station who survey the in situ instruments, check the data quality and transfer to the databases. In situ data were extracted from the EBAS database (http://ebas.nilu.no/default.aspx; Tørseth et al. (2012)).

Appendix A. Supplementary data

Supplementary data to this article can be found online at https://doi.org/10.1016/j.atmosres.2023.107043.

References

Ackermann, J., 1998. The extinction-to-backscatter ratio of tropospheric aerosol: a numerical study. J. Atmos. Ocean. Technol. 15 (4), 1043–1050. https://doi.org/10.1175/1520-0426(1998)015<1043:TETBRO>2.0.CO;2.

Alados-Arboledas, L., Müller, D., Guerrero-Rascado, J.L., Navas-Guzmán, F., Pérez-Ramírez, D., Olmo, F.J., 2011. Optical and microphysical properties of fresh biomass burning aerosol retrieved by Raman lidar, and star- and sun photometry. Geophys. Res. Lett. 38, L01807 https://doi.org/10.1029/2010GL045999.

Ancellet, G., Pelon, J., Totems, J., Chazette, P., Bazureau, A., Sicard, M., Di Iorio, T., Dulac, F., Mallet, M., M., 2016. Long-range transport and mixing of aerosol sources during the 2013 North American biomass burning episode: Analysis of multiple lidar observations in the western Mediterranean basin. Atmos. Chem. Phys. 16 (7), 4725–4742. https://doi.org/10.5194/acp-16-4725-2016.

Baray, J.-L., Bah, A., Cacault, P., Sellegri, K., Pichon, J.-M., Deguillaume, L., Montoux, N., Noel, V., Seze, G., Gabarrot, F., et al., 2019. Cloud occurrence frequency at Puy de Dôme (France) deduced from an automatic camera image analysis: method, validation, and comparisons with larger scale parameters. Atmosphere (Basel) 10 (12), 808. https://doi.org/10.3390/atmos10120808.

Baray, J.L., Deguillaume, L., Colomb, A., Sellegri, K., Freney, E., Rose, C., Van Baelen, J., Pichon, J.M., Picard, D., Fréville, P., et al., 2020. Cézeaux-Aulnat-Opme-Puy de Dôme: a multi-site for the long-term survey of the tropospheric composition and climate change. Atmos. Meas. Tech. 13 (6), 3413–3445. https://doi.org/10.5194/amt-13-3413-2020.

Berjon, A., Barreto, A., Hernández, Y., Yela, M., Toledano, C., Cuevas, E., 2019. A 10-year characterization of the Saharan Air Layer lidar ratio in the subtropical North Atlantic. Atmos. Chem. Phys. 19 (9), 6331–6349. https://doi.org/10.5194/acp-19-6331-2019.

Bezdĕk, A., Sebera, J., 2013. Matlab script for 3D visualizing geodata on a rotating globe. Comput. Geosci. 56, 127–130. https://doi.org/10.1016/j.cageo.2013.03.007.

Bourcier, L., Sellegri, K., Chausse, P., Pichon, J.M., Laj, P., 2012. Seasonal variation of water-soluble inorganic components in aerosol size-segregated at the puy de Dôme

station (1,465 m a.s.l.), France. J. Atmos. Chem. 69 (1), 47–66. https://doi.org/10.1007/s10874-012-9229-2.
Boyouk, N., Léon, J.F., Delbarre, H., Augustin, P., Fourmentin, M., 2011. Impact of sea breeze on vertical structure of aerosol optical properties in Dunkerque, France. Atmos. Res. 101 (4), 902–910. https://doi.org/10.1016/j.atmosres.2011.05.016.
Bréon, F.-M., 2013. Aerosol extinction-to-backscatter ratio derived from passive satellite measurements. Atmos. Chem. Phys. 13 (17), 8947–8954. https://doi.org/10.5194/acp-13-8947-2013.
Burkart, J., Steiner, G., Reischl, G., Moshammer, H., Neuberger, M., Hitzenberger, R., 2010. Characterizing the performance of two optical particle counters (Grimm OPC1.108 and OPC1.109) under urban aerosol conditions. J. Aerosol Sci. 41 (10), 953–962. https://doi.org/10.1016/j.jaerosci.2010.07.007.
Burton, S.P., Ferrare, R.A., Hostetler, C.A., Hair, J.W., Rogers, R.R., Obland, M.D., Butler, C.F., Cook, A.L., Harper, D.B., Froyd, K.D., 2012. Aerosol classification using airborne High Spectral Resolution Lidar measurements – methodology and examples. Atmos. Meas. Tech. 5 (1), 73–98. https://doi.org/10.5194/amt-5-73-2012.
Burton, S.P., Ferrare, R.A., Vaughan, M.A., Omar, A.H., Rogers, R.R., Hostetler, C.A., Hair, J.W., 2013. Aerosol classification from airborne HSRL and comparisons with the CALIPSO vertical feature mask. Atmos. Meas. Tech. 6, 1397–1412. https://doi.org/10.5194/amt-6-1397-2013.
Cattrall, C., Reagan, J., Thome, K., Dubovik, O., 2005. Variability of aerosol and spectral lidar and backscatter and extinction ratios of key aerosol types derived from selected aerosol robotic network locations. J. Geophys. Res. Atmos. 110 (D10) https://doi.org/10.1029/2004JD005124.
Chauvigné, A., Sellegri, K., Hervo, M., Montoux, N., Freville, P., Goloub, P., 2016. Comparison of the aerosol optical properties and size distribution retrieved by sun photometer with in situ measurements at midlatitude. Atmos. Meas. Tech. 9 (9), 4569–4585. https://doi.org/10.5194/amt-9-4569-2016.
Chazette, P., Royer, P., 2017. Springtime major pollution events by aerosol over Paris Area: from a case study to a multiannual analysis. J. Geophys. Res. Atmos. 122, 8101–8119. https://doi.org/10.1002/2017JD026713.
Chýlek, P., Srivastava, V., Pinnick, R.G., Wang, R.T., 1988. Scattering of electromagnetic waves by composite spherical particles: experiment and effective medium approximations. Appl. Opt. 27, 2396–2404. https://doi.org/10.1364/AO.27.002396.
Dagsson-Waldhauserova, P., Arnalds, O., Olafsson, H., 2017. Long-term dust aerosol production from natural sources in Iceland. J. Air Waste Manage. Assoc. 67 (2), 173–181. https://doi.org/10.1080/10962247.2013.805703.
Evans, B.T.N., 1988. Sensitivity of the backscatter/extinction ratio to changes in aerosol properties: implications for lidar. Appl. Opt. 27 (15), 3299. https://doi.org/10.1364/AO.27.003299.
Farah, A., Freney, E., Chauvigné, A., Baray, J.L., Rose, C., Picard, D., Colomb, A., Hadad, D., Abboud, M., Farah, W., Sellegri, K., 2018. Seasonal variation of aerosol size distribution data at the PUY de Dôme station with emphasis on the boundary layer/free troposphere segregation. Atmosphere (Basel) 9 (7). https://doi.org/10.3390/atmos9070244.
Farah, A., Freney, E., Canonaco, F., Prévôt, A.S.H., Pichon, J.M., Abboud, M., Farah, W., Sellegri, K., 2021. Altitude aerosol measurements in central France: seasonality, sources and free-troposphere/boundary layer segregation. Earth Sp. Sci. https://doi.org/10.1029/2019EA001018 n/a (n/a):e2019EA001018.
Feng, X., Wang, J., Teng, S., Xu, X., Zhu, B., Zhu, X., Yurkin, M.A., Liu, C., 2021. Can light absorption of black carbon still be enhanced by mixing with absorbing materials? Atmos. Environ. 118358 https://doi.org/10.1016/j.atmosenv.2021.118358.
Ferrare, R.A., Turner, D.D., Brasseur, L.H., Feltz, W.F., Dubovik, O., Tooman, T.P., 2001. Raman lidar measurements of the aerosol extinction-to-backscatter ratio over the Southern Great Plains. J. Geophys. Res. Atmos. 106 (D17), 20333–20347. https://doi.org/10.1029/2000JD000144.
Flores, M.J., Bar-Or, R.Z., Bluvshtein, N., Abo-Riziq, A., Kostinski, A., Borrmann, S., Koren, I., Rudich, Y., 2012. Absorbing aerosols at high relative humidity: linking hygroscopic growth to optical properties. Atmos. Chem. Phys. 12 (12), 5511–5521. https://doi.org/10.5194/acp-12-5511-2012.
Forster, P., Storelvmo, T., Armour, K., Collins, W., Dufresne, J.-L., Frame, D., Lunt, D.J., Mauritsen, T., Palmer, M.D., Watanabe, M., et al., 2021. The Earth's energy budget, climate feedbacks, and climate sensitivity. In: Masson-Delmotte, V., Zhai, P., Pirani, A., Connors, S.L., Péan, C., Berger, S., Caud, N., Chen, Y., Goldfarb, L., Gomis, M.I., Huang, M., Leitzell, K., Lonnoy, E., Matthews, J.B.R., Maycock, T.K., Waterfield, T., Yelekçi, O., Yu, R., Zhou, B. (Eds.), Climate Change 2021: The Physical Science Basis. Contribution of Working Group I to the Sixth Assessment Report of the Intergovernmental Panel on Climate Change. Cambridge University Press, Cambridge, United Kingdom and New York, NY, USA, pp. 923–1054. https://doi.org/10.1017/9781009157896.009.
Freney, E.J., Sellegri, K., Canonaco, F., Boulon, J., Hervo, M., Weigel, R., Pichon, J.M., Colomb, A., Prévôt, A.S.H., Laj, P., 2011. Seasonal variations in aerosol particle composition at the puy-de-Dôme research station in France. Atmos. Chem. Phys. 11 (24), 13047–13059. https://doi.org/10.5194/acp-11-13047-2011.
Fröhlich, R., Cubison, M.J., Slowik, J.G., Bukowiecki, N., Prévôt, A.S.H., Baltensperger, U., Schneider, J., Kimmel, J.R., Gonin, M., Rohner, U., et al., 2013. The ToF-ACSM: a portable aerosol chemical speciation monitor with TOFMS detection. Atmos. Meas. Tech. 6 (11), 3225–3241. https://doi.org/10.5194/amt-6-3225-2013.
Groß, S., Esselborn, M., Weinzierl, B., Wirth, M., Fix, A., Petzold, A., 2013. Aerosol classification by airborne high spectral resolution lidar observations. Atmos. Chem. Phys. 13 (5), 2487–2505. https://doi.org/10.5194/acp-13-2487-2013.
Haarig, M., Ansmann, A., Baars, H., Jimenez, C., Veselovskii, I., Engelmann, R., Althausen, D., 2018. Depolarization and lidar ratios at 355, 532, and 1064 nm and microphysical properties of aged tropospheric and stratospheric Canadian wildfire smoke. Atmos. Chem. Phys. 18, 11847–11861. https://doi.org/10.5194/acp-18-11847-2018.
Hervo, M., Sellegri, K., Pichon, J.-M., Roger, J.C., Laj, P., 2014. Long term measurements of optical properties and their hygroscopic enhancement. Atmos. Chem. Phys. Discuss. 14 (20), 27731–27767. https://doi.org/10.5194/acpd-14-27731-2014.
Highwood, E.J., Northway, M.J., McMeeking, G.R., Morgan, W.T., Liu, D., Osborne, S., Bower, K., Coe, H., Ryder, C., Williams, P., 2012. Aerosol scattering and absorption during the EUCAARI-LONGREX flights of the Facility for Airborne Atmospheric Measurements (FAAM) BAe-146: can measurements and models agree? Atmos. Chem. Phys. 12 (15), 7251–7267. https://doi.org/10.5194/acp-12-7251-2012.
Holmgren, H., Sellegri, K., Hervo, M., Rose, C., Freney, E., Villani, P., Laj, P., 2014. Hygroscopic properties and mixing state of aerosol measured at the high-altitude site Puy de Dôme (1465 m a.s.l.), France. Atmos. Chem. Phys. 14 (18), 9537–9554. https://doi.org/10.5194/acp-14-9537-2014.
Janicka, L., Stachlewska, I.S., 2019. Properties of biomass burning aerosol mixtures derived at fine temporal and spatial scales from Raman lidar measurements: part I optical properties. Atmos. Chem. Phys. Discuss. 2019, 1–46. https://doi.org/10.5194/acp-2019-207.
Josset, D., Rogers, R., Pelon, J., Hu, Y., Liu, Z., Omar, A., Zhai, P.-W., 2011. CALIPSO lidar ratio retrieval over the ocean. Opt. Express 19 (19), 18696. https://doi.org/10.1364/oe.19.018696.
Kim, M.H., Kim, S.W., Yoon, S.C., Omar, A.H., 2013. Comparison of aerosol optical depth between CALIOP and MODIS-Aqua for CALIOP aerosol subtypes over the ocean. J. Geophys. Res. Atmos. 118 (23), 13,241–13,252. https://doi.org/10.1002/2013JD019527.
Kim, M.H., Omar, A.H., Tackett, J.L., Vaughan, M.A., Winker, D.M., Trepte, C.R., Hu, Y., Liu, Z., Poole, L.R., Pitts, M.C., el al., 2018. The CALIPSO version 4 automated aerosol classification and lidar ratio selection algorithm. Atmos. Meas. Tech. 11 (11), 6107–6135. https://doi.org/10.5194/amt-11-6107-2018.
Kim, M.H., Kim, S.W., Omar, A.H., 2020. Dust lidar ratios retrieved from the CALIOP measurements using the MODIS AOD as a constraint. Remote Sens. 12 (2) https://doi.org/10.3390/rs12020251.
Laj, P., Bigi, A., Rose, C., Andrews, E., Lund Myhre, C., Collaud Coen, M., Lin, Y., Wiedensohler, A., Schultz, M., Ogren, J.A., et al., 2020. A global analysis of climate-relevant aerosol properties retrieved from the network of Global Atmosphere Watch (GAW) near-surface observatories. Atmos. Meas. Tech. 13, 4353–4392. https://doi.org/10.5194/amt-13-4353-2020.
Liu, D., Wang, Z., Liu, Z., Winker, D., Trepte, C., 2008. A height resolved global view of dust aerosols from the first year CALIPSO lidar measurements. J. Geophys. Res. 113, D16214 https://doi.org/10.1029/2007JD009776.
Mallet, M., Roger, J.C., Despiau, S., Putaud, J.P., Dubovik, O., 2004. A study of the mixing state of black carbon in urban zone. J. Geophys. Res. Atmos. 109 (D4) https://doi.org/10.1029/2003JD003940 n/a-n/a.
Masonis, S.J., Anderson, T.L., Covert, D.S., Kapustin, V., Clarke, A.D., Howell, S., Moore, K., 2003. A study of the extinction-to-backscatter ratio of marine aerosol during the shoreline environment aerosol study. J. Atmos. Ocean. Technol. 20 (10), 1388–1402. https://doi.org/10.1175/1520-0426(2003)020<1388:ASOTER>2.0.CO;2.
Mätzler, C., 2002. MATLAB Functions for Mie Scattering and Absorption. IAP Res Rep 2002–08 (July 2002), pp. 1139–1151. https://doi.org/10.1039/b811392k.
McAuliffe, M.A.P., Ruth, A.A., 2013. Typical tropospheric aerosol backscatter profiles for Southern Ireland: the Cork Raman lidar. Atmos. Res. 120–121, 334–342. https://doi.org/10.1016/j.atmosres.2012.09.020.
Mona, L., Amodeo, A., Pandolfi, M., Pappalardo, G., 2006. Saharan dust intrusions in the Mediterranean area: three years of Raman lidar measurements. J. Geophys. Res. 111 (D16), D16203 https://doi.org/10.1029/2005JD006569.
Müller, D., Ansmann, A., Mattis, I., Tesche, M., Wandinger, U., Althausen, D., Pisani, G., 2007. Aerosol-type-dependent lidar ratios observed with Raman lidar. J. Geophys. Res. 112 (D16), D16202 https://doi.org/10.1029/2006JD008292.
Müller, T., Henzing, J.S., De Leeuw, G., Wiedensohler, A., Alastuey, A., Angelov, H., Bizjak, M., Collaud Coen, M., Engström, J.E., Gruening, C., et al., 2011. Characterization and intercomparison of aerosol absorption photometers: result of two intercomparison workshops. Atmos. Meas. Tech. 4 (2), 245–268. https://doi.org/10.5194/amt-4-245-2011.
Mylonaki, M., Giannakaki, E., Papayannis, A., Papanikolaou, C.-A., Komppula, M., Nicolae, D., Papagiannopoulos, N., Amodeo, A., Baars, H., Soupiona, O., 2021. Aerosol type classification analysis using EARLINET multiwavelength and depolarization lidar observations. Atmos. Chem. Phys. 21 (3), 2211–2227. https://doi.org/10.5194/acp-21-2211-2021.
Navas-Guzmán, F., Bravo-Aranda, J.A., Guerrero-Rascado, J.L., Granados-Muñoz, M.J., Alados-Arboledas, L., 2013. Statistical analysis of aerosol optical properties retrieved by Raman lidar over Southeastern Spain. Tellus Ser. B Chem. Phys. Meteorol. 65 (1) https://doi.org/10.3402/tellusb.v65i0.21234.
Nicolae, V., Talianu, C., Andrei, S., Antonescu, B., Ene, D., Nicolae, D., Dandocsi, A., Toader, V.-E., Ștefan, S., Savu, T., et al., 2019. Multiyear typology of long-range transported aerosols over Europe. Atmosphere (Basel) 10 (9), 482. https://doi.org/10.3390/atmos10090482.
Omar, A.H., Winker, D.M., Kittaka, C., Vaughan, M.A., Liu, Z., Hu, Y., Trepte, C.R., Rogers, R.R., Ferrare, R.A., Lee, K.P., et al., 2009. The CALIPSO automated aerosol classification and lidar ratio selection algorithm. J. Atmos. Ocean. Technol. 26 (10), 1994–2014. https://doi.org/10.1175/2009JTECHA1231.1.
Pedros, R., Estelles, V., Sicard, M., Gomez-Amo, J.L., Utrillas, M.P., Martinez-Lozano, J. A., Rocadenbosch, F., Perez, C., Recio, J.M.B., 2010. Climatology of the aerosol extinction-to-backscatter ratio from sun-photometric measurements. IEEE Trans.

Geosci. Remote Sens. 48 (1), 237–249. https://doi.org/10.1109/TGRS.2009.2027699.
Petzold, A., Schönlinner, M., 2004. Multi-angle absorption photometry—a new method for the measurement of aerosol light absorption and atmospheric black carbon. J. Aerosol Sci. 35 (4), 421–441. https://doi.org/10.1016/j.jaerosci.2003.09.005.
Prospero, J.M., Bullard, J.E., Hodgkins, R., 2012. High-latitude dust over the North Atlantic: inputs from icelandic proglacial dust storms. Science 335 (6072), 1078–1082. https://doi.org/10.1126/science.1217447.
Pye, H.O.T., Nenes, A., Alexander, B., Ault, A.P., Barth, M.C., Clegg, S.L., Collett Jr., J.L., Fahey, K.M., Hennigan, C.J., Herrmann, H., et al., 2020. The acidity of atmospheric particles and clouds. Atmos. Chem. Phys. 20 (8), 4809–4888. https://doi.org/10.5194/acp-20-4809-2020.
Raut, J.-C., Chazette, P., 2007. Retrieval of aerosol complex refractive index from a synergy between lidar, sunphotometer and in situ measurements during LISAIR experiment. Atmos. Chem. Phys. 7, 2797–2815. https://doi.org/10.5194/acp-7-2797-2007.
Rose, C., Boulon, J., Hervo, M., Holmgren, H., Asmi, E., Ramonet, M., Laj, P., Sellegri, K., 2013. Long-term observations of cluster ion concentration, sources and sinks in clear sky conditions at the high-altitude site of the Puy de Dôme, France. Atmos. Chem. Phys. 13 (22), 11573–11594. https://doi.org/10.5194/acp-13-11573-2013.
Russell, P.B., Bergstrom, R.W., Shinozuka, Y., Clarke, A.D., DeCarlo, P.F., Jimenez, J.L., Livingston, J.M., Redemann, J., Dubovik, O., Strawa, A., 2010. Absorption Angstrom Exponent in AERONET and related data as an indicator of aerosol composition. Atmos. Chem. Phys. 10 (3), 1155–1169. https://doi.org/10.5194/acp-10-1155-2010.
Santese, M., De Tomasi, F., Perrone, M.R., 2008. Advection patterns and aerosol optical and microphysical properties by AERONET over south-East Italy in the Central Mediterranean. Atmos. Chem. Phys. 8 (7), 1881–1896. https://doi.org/10.5194/acp-8-1881-2008.
Schuster, G.L., Vaughan, M., MacDonnell, D., Su, W., Winker, D., Dubovik, O., Lapyonok, T., Trepte, C., 2012. Comparison of CALIPSO aerosol optical depth retrievals to AERONET measurements, and a climatology for the lidar ratio of dust. Atmos. Chem. Phys. 12 (16), 7431–7452. https://doi.org/10.5194/acp-12-7431-2012.
Sellegri, K., Laj, P., Marinoni, A., Dupuy, R., Legrand, M., Preunkert, S., 2003. Contribution of gaseous and particulate species to droplet solute composition at the Puy de Dôme, France. Atmos. Chem. Phys. 3 (5), 1522.
Shin, S.K., Tesche, M., Kim, K., Kezoudi, M., Tatarov, B., Müller, D., Noh, Y., 2018. On the spectral depolarisation and lidar ratio of mineral dust provided in the AERONET version 3 inversion product. Atmos. Chem. Phys. 18 (17), 12735–12746. https://doi.org/10.5194/acp-18-12735-2018.
Soupiona, O., Samaras, S., Ortiz-Amezcua, P., Böckmann, C., Papayannis, A., Moreira, G. A., Benavent-Oltra, J.A., Guerrero-Rascado, J.L., Bedoya-Velásquez, A.E., Olmo, F.J., et al., 2019. Retrieval of optical and microphysical properties of transported Saharan dust over Athens and Granada based on multi-wavelength Raman lidar measurements: study of the mixing processes. Atmos. Environ. 214 https://doi.org/10.1016/j.atmosenv.2019.116824.
Tao, W.-K., Chen, J.-P., Li, Z., Wang, C., Zhang, C., 2012. Impact of aerosols on convective clouds and precipitation. Rev. Geophys. 50 (2) https://doi.org/10.1029/2011RG000369.
Tesche, M., Ansmann, A., Müller, D., Althausen, D., Mattis, I., Heese, B., Freudenthaler, V., Wiegner, M., Esselborn, M., Pisani, G., et al., 2009. Vertical profiling of Saharan dust with Raman lidars and airborne HSRL in southern Morocco during SAMUM. Tellus Ser. B Chem. Phys. Meteorol. 61 (1), 144–164. https://doi.org/10.1111/j.1600-0889.2008.00390.x.
Tomasi, C., Kokhanovsky, A.A., Lupi, A., Ritter, C., Smirnov, A., O'Neill, N.T., Stone, R. S., Holben, B.N., Nyeki, S., Wehrli, C., et al., 2015. Aerosol remote sensing in polar regions. Earth-Sci. Rev. 140, 108–157. https://doi.org/10.1016/j.earscirev.2014.11.001.
Tørseth, K., Aas, W., Breivik, K., Fjæraa, A.M., Fiebig, M., Hjellbrekke, A.G., Lund Myhre, C., Solberg, S., Yttri, K.E., 2012. Introduction to the European Monitoring and Evaluation Programme (EMEP) and observed atmospheric composition change during 1972–2009. Atmos. Chem. Phys. 12 (12), 5447–5481. https://doi.org/10.5194/acp-12-5447-2012.
Vaughan, G., Draude, A.P., Ricketts, H.M.A., Schultz, D.M., Adam, M., Sugier, J., Wareing, D.P., 2018. Transport of Canadian forest fire smoke over the UK as observed by lidar. Atmos. Chem. Phys. 18 (15), 11375–11388. https://doi.org/10.5194/acp-18-11375-2018.
Venzac, H., Sellegri, K., Villani, P., Picard, D., Laj, P., 2009. Seasonal variation of aerosol size distributions in the free troposphere and residual layer at the puy de Dôme station, France. Atmos. Chem. Phys. 9 (4), 1465–1478. https://doi.org/10.5194/acp-9-1465-2009.
Veselovskii, I., Hu, Q., Goloub, P., Podvin, T., Korenskiy, M., Derimian, Y., Legrand, M., Castellanos, P., 2020. Variability in lidar-derived particle properties over West Africa due to changes in absorption: towards an understanding. Atmos. Chem. Phys. 20 (11), 6563–6581. https://doi.org/10.5194/acp-20-6563-2020.
von Hoyningen-Huene, W., Schmidt, T., Schienbein, S., Kee, C.A., Tick, L.J., 1999. Climate-relevant aerosol parameters of South-East-Asian forest fire haze. Atmos. Environ. 33 (19), 3183–3190. https://doi.org/10.1016/S1352-2310(98)00422-1.
Wang, Y., Jiang, J.H., Su, H., 2015. Atmospheric responses to the redistribution of anthropogenic aerosols. J. Geophys. Res. Atmos. 120 (18), 9625–9641. https://doi.org/10.1002/2015JD023665.
Wang, S.-H., Lei, H.-W., Pani, S.K., Huang, H.-Y., Lin, N.-H., Welton, E.J., Chang, S.-C., Wang, Y.-C., 2020. Determination of lidar ratio for major aerosol types over Western North Pacific based on long-term MPLNET data. Remote Sens. 12, 2769. https://doi.org/10.3390/rs12172769.
Wiegner, M., Groß, S., Freudenthaler, V., Schnell, F., Gasteiger, J., 2011. The May/June 2008 Saharan dust event over Munich: intensive aerosol parameters from lidar measurements. J. Geophys. Res. Atmos. 116 (D23) https://doi.org/10.1029/2011JD016619 n/a-n/a.
Winker, D.M., Pelon, J., Coakley, J.A., Ackerman, S.A., Charlson, R.J., Colarco, P.R., Flamant, P., Fu, Q., Hoff, R.M., Kittaka, C., et al., 2010. The CALIPSO mission: a global 3D view of aerosols and clouds. Bull. Am. Meteorol. Soc. 91 (9), 1211–1229. https://doi.org/10.1175/2010BAMS3009.1.
Zhang, X., Mao, M., Yin, Y., 2019. Optically effective complex refractive index of coated black carbon aerosols: from numerical aspects. Atmos. Chem. Phys. 19 (11), 7507–7518. https://doi.org/10.5194/acp-19-7507-2019.
Zhang, X., Mao, M., Chen, H., 2020. Characterization of optically effective complex refractive index of black carbon composite aerosols. J. Atmos. Solar-Terrestrial Phys. 198 (December 2019), 105180. https://doi.org/10.1016/j.jastp.2019.105180.